Iraqi Journal of Physics, 2021
DOI: 10.30723/ijp.v19i51.685

Vol.19, No.51, PP.41-53
P-ISSN: 2070-4003
E-ISSN: 2664-5548

Impact of Aluminum Oxide Content on the Structural and Optical Properties of ZnO: AlO Thin Films

Hawraa H. Abbas[a*], Bushra A. Hasan[b]
Department of Physics, College of Science, University of Baghdad, Baghdad, Iraq
[b]Email: bushra_abhasan@yahoo.com
[a*]Corresponding author: Hawraa.Abbas1204@sc.uobaghdad.edu.iq

Abstract

AlO-doped ZnO nanocrystalline thin films from with nano crystallite size in the range (19-15 nm) were fabricated by pulsed laser deposition technique. The reduction of crystallite size by increasing of doping ratio shift the bandgap to IR region the optical band gap decreases in a consistent manner, from 3.21to 2.1 eV by increasing AlO doping ratio from 0 to 7wt% but then returns to grow up to 3.21 eV by a further increase the doping ratio. The bandgap increment obtained for 9% AlO dopant concentration can be clarified in terms of the Burstein–Moss effect whereas the aluminum donor atom increased the carrier's concentration which in turn shifts the Fermi level and widened the bandgap (blue-shift). The engineering of the bandgap by low concentration of AlO dopant makes ZnO: AlO thin films favorable for the fabrication of optoelectronic devices. The optical constants were calculated and was found to be greatly affected by the increasing the doping ratio.

Article info.

Keywords:
ZnO: AlO thin films, energy gap, X-ray diffraction, Optical properties, pulsed laser deposition PLD.

Article history:
Received: Jun. 14, 2021
Accepted: Aug. 12, 2021
Published: Dec. 01, 2021

1. Introduction

ZnO bandgap technology provides continuous development of transparent photonic devices, transparent electronics and transparent electrodes. [1–3]. ZnO also provides acoustic surface wave equipment [4]. solar cells, [5], flat panel display etc. [6]. In dye-sensitized solar cells, a transparent conducting layer of doped ZnO nano-film is used [7]. In applications such as energy yield, flexible electronics, nanowires with ZnO also show good performance [8]. ZnO has abroad direct bandgap of about 3.37 eV which makes it optically transparent in the visible spectrum. It also has photoluminescence properties due to its high exciton binding energy of 60 meV at room temperature [9]. Regardless of the fabrication conditions and methods, ZnO emits a blue-green emission at room temperature. Surface defects, such as singly ionized oxygen vacancies, Zn interstitials, and Zn vacancies, are believed to be responsible for the green photoluminescence of ZnO structures [10]. Zinc oxide can be used to expand a variety of nanostructures. Flame transport synthesis (FTS)-fabricated ZnO tetrapods and networks display promising photocatalytic and photoswitching properties. The network of these structures has enticing properties including high-temperature stability, electrical conductivity, tunable Young's modulus, and so on, which open up a wide range of possibilities in both basic research and industrial applications. SnO_2 nano- and microstructures, in addition to ZnO [11]. The FTS can also make a variety of other metal oxides [12].

Due to deep level defects, a sample with direct integration of ZnO nano- and micro-needles using FTS shows NBE emission about 380 nm and a broad green

Iraqi Journal of Physic is licensed under a Creative Commons Attribution 4.0 International License

luminescence [13]. Isoelectronic dopants, such as Ca, Mg, and Sr have been used to tune the bandgap of ZnO, while Group III metal dopants, such as Fe, have been used to tune the bandgap of ZnO. To improve the electrical conductivity and transparency of ZnO films, Al, In, and Ga have been added as required [14–16]. Aluminum has proven to be the most efficient of these dopants in producing high-quality samples with improved clarity to visible light and emission in the UV/blue field [17]. As a consequence of the Burstein-Moss effect, the band distance is also altered (BM). Because of its naturally occurring n-type conductivity and optical clarity, zinc oxide is emerging as a potential alternative to ITO for thin-film transparent electrode applications. Thermally and mechanically, doped ZnO films are said to be more stable [18–22]. PLD sputtering; thermal evaporation, and magnetron sputtering, are some of the physical deposition methods that can be used [23]. Chemical vapor deposition and wet chemical routes are examples of situations where maintaining a vacuum is important [24–29]. Spray pyrolysis, is a wet chemical route for large-area deposition that does not require vacuum. It is also used to synthesize Al-doped ZnO films. It was found that the surface morphology of ZnO-based films has a major impact on their optical properties [30]. Apart from studying the structure and surface of the film, doping impact on optical properties such as transmission, bandgap, and optical constants, is the primary subject of this research paper.

2. Experimental work

ZnO and AlO with high purity 99.99 % supplied from Aldrich Company were the materials used in the present work. The starting materials which used to prepare different composites with various concentrations were weighed according to the following ratios (100/0, 97/3, 95/5, 93/7, and 91/9 % using an electronic balance with four digits after the point (10^{-4} gm). The composites were subjected to a sintering process by putting the composites in quartz ampoule of length ~ 25 cm and internal diameter ~ 8 mm which was evacuated to ~10^{-3} Torr and sealed. The ampoules were put in an oven at 1273K for 5 hours. The obtained composites were grounded to obtain a powder which was pressed, with a hydraulic piston type (SPECIAL), under pressure of 7 tons for 15 sec, to form pellets with a diameter of 1 cm and of 0.5 cm thickness. ZnO: AlO composite was used to prepare thin films using pulsed laser deposition technique. The deposition was done in a vacuum of $2x10^{-2}$ Torr using Nd: YAG laser beam (with 500mJ energy, 500 pulse, and frequency of 6Hz) which was focused through a window an incident on the target. The ablated atoms were incident on the glass substrates and get gathered to create thin films. The optical interferometer method was used to determine the film thickness (t). The XRD measurements were carried out with a diffractometer (type XRD / 6000 Shimadzu) at (the Iranian Republic Laboratories) using Cu-Kα (λ=1.5404A^{o}) radiation operating at 30 kV and 20 mA.

3. Results and discussion

Fig.2 shows the x-ray diffraction spectra of the hexagonal wurtzite structure of ZnO according to the standard JCPDS cards PDF#36-1451 which exhibit remarkable orientation along (100), (002) and (101) plane with the (100) plane as the predominate plane for crystal growth. This result is similar to that of Srivastava et al. [31]. No impurity was observed in the thin films that have been doped. The peak along, the a-axis, i.e. (100) plane are located at 2θ=32.0357°, 32.0714°, 32.0357°, 31.9543 and 32.0357° for samples (ZnO), (ZnO:3%wt.AlO), (ZnO:5%wt.AlO), (ZnO:7%wt.AlO), and (ZnO:9%wt.AlO) respectively. The diffraction peak, was

shifts, to a higher value of 2θ, for ZnO:3%wt. AlO and ZnO:7%wt. AlO and exceeded the angle of undoped ZnO.

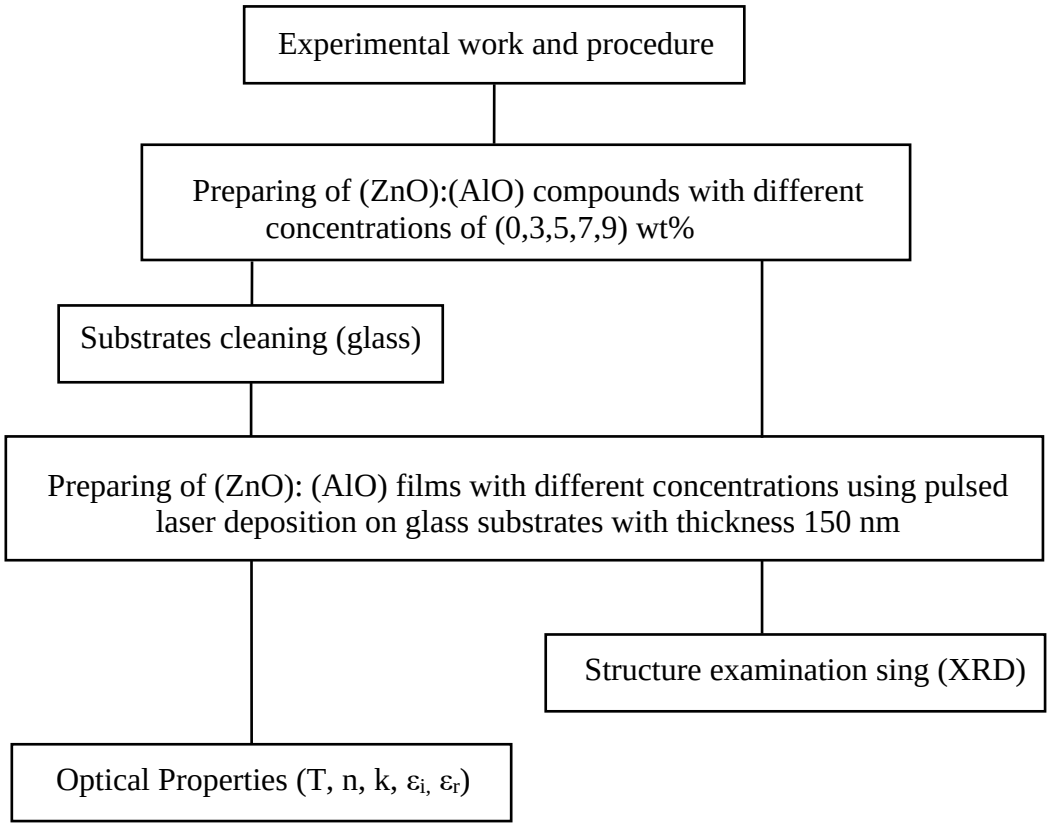

Figure 1: The scheme of the experimental work.

The Scherrer formula was used to measure the average crystal size (D):

$$D = \frac{0.9\lambda}{\beta \cos\theta} \quad (1)$$

where β and θ are the full widths at half maximum and the glancing angle respectively. The dislocation density Δ and the strain δ were determined by applying the following relations, respectively [32]:

$$\delta = \frac{1}{D^2} \quad (2)$$

and

$$\Delta = \frac{D \cos\theta \frac{\delta}{2}}{4} \quad (3)$$

The estimated crystallite size using Debye-Scherer relation varies from growing up to 19 nm as AlO was introduced to the host oxide but it reached lower value of 15 nm at the doping ratio of 7%wt. The dislocation density and the strain values were also calculated. The strain value was found to range from 19×10^{-4} to 22×10^{-4} as the composite ratio was varied from 0 to 7wt%. Strain in sample ZnO:3%wt. AlO was less than residual samples. This reflects the higher crystallite size.

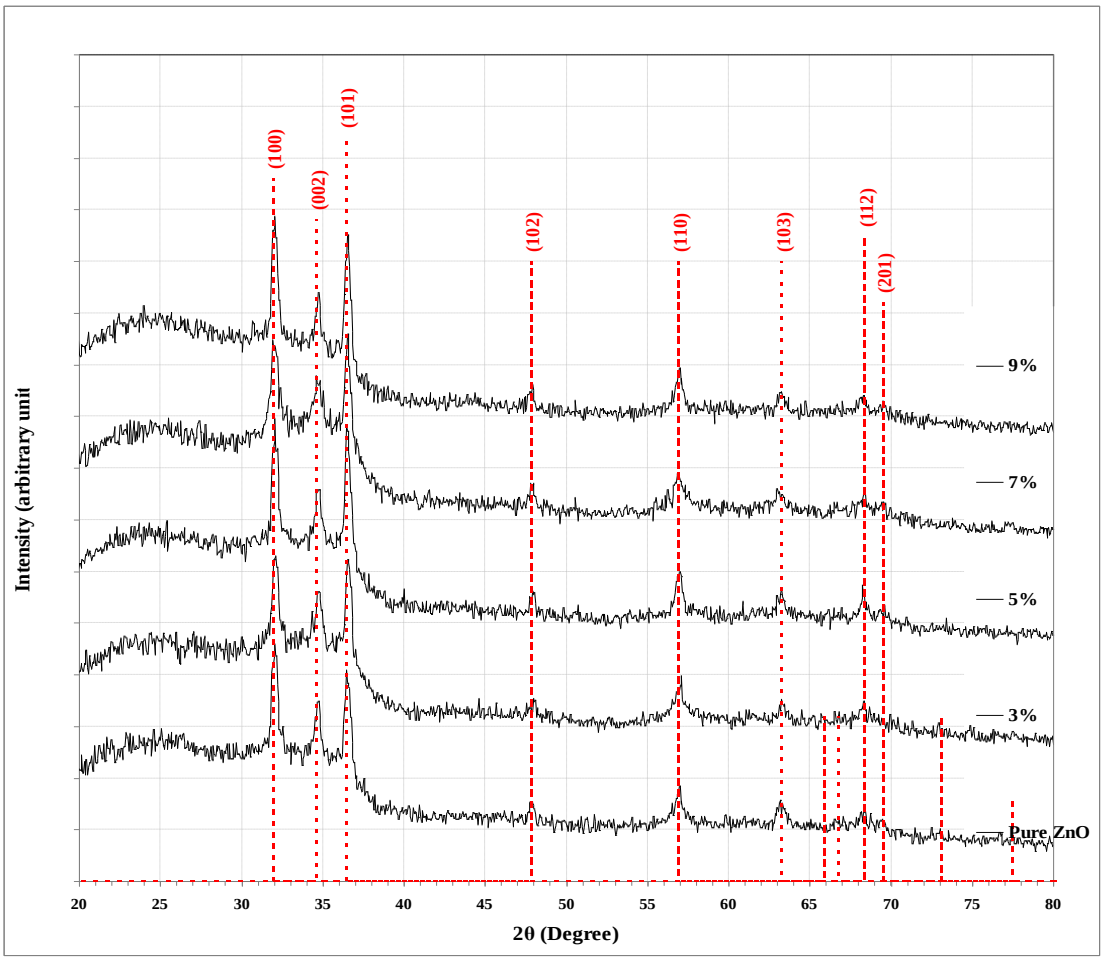

Figure 2: The diffraction pattern of ZnO: AlO thin films.

When ZnO crystallizes as wurtzite, the oxygen atoms are organized in a hexagonal close packed form, with zinc atoms occupying half of the tetrahedral positions. The atoms Zn and O are tetrahedrally coupled to one other and hence share the same location. All of the octahedral and half of the tetrahedral sites in the zinc structure are vacant. Bragg's law states that [32],

$$n\lambda=2\,d\,\sin\theta \qquad (4)$$

where n denotes the diffraction order (typically n = 1), X is the X-ray wavelength, and d denotes the distance between planes with the given Miller indices h, k, and l.

The plane spacing d is related to the lattice constants a, c, and the Miller indices in the ZnO hexagonal structure by the following relationship [32],

$$1/d^2=4/3(h^2+hk+k^2)/a^2+(l^2/c^2) \qquad (5)$$

for the first-order approximation:

$$(n=1);\ \sin^2\theta=\lambda^2/2a^2[4/3(h^2+hk+k^2)+(a/c)l^2] \qquad (6)$$

The lattice constant a for the (100) plane is determined by the relation,

$$a=\lambda/\sqrt{3}\sin\theta \qquad (7)$$

While, the lattice constant c for the (002) plane is determined by the relation,

$$c=\lambda/\sin\theta \qquad (8)$$

The a-lattice constant is used here, was seen to be decreasing for the samples ZnO:3 wt%. AlO (AZ3) but remained constant for the samples ZnO:5wt%. AlO (AZ5) and ZnO:9wt%. AlO (AZ9). The c-lattice constant, decreased for samples ZnO:3wt%. AlO (AZ3), ZnO:7wt%. AlO (AZ7), and ZnO:9wt%. AlO (AZ9), and grew up for sample ZnO:5wt%. AlO (AZ5). The amount of defect states in the prepared thin films which represents dislocation density increased randomly from $3.15x10^{15}$ to $4.2x10^{15}$lines/m^2 for the undoped and doped ZnO:9 wt%. AlO (AZ7) samples. Table 1 shown the results of x-ray diffraction.

The decrease of c- lattice constant indicates that doping ZnO with AlO results from the shrinkage of the lattice constant while the growing of c-lattice constant indicates that the dopant atoms Al^{3+} continue to interstitial habitation. A similar mode was found for calcium-doped zinc oxide films [33]. This behavior was ascribed to the high difference in ionic radii of dopant atoms Al^{3+}. Al^{3+}, having a significantly reduced size (r_{Zn}^{2+} = 0.074 nm and r_{Al}^{3+} = 0.054 nm) [34-37].

Table 1: The results of x-ray diffraction on ZnO: AlO thin films.

AlO wt%	2θ (Deg.)	FWHM (Deg.)	d_{hkl} Exp. (Å)	C.S (nm)	hkl	d_{hkl} Std. (Å)	δ ×10^{15} (line/m^2)	strain
	32.0357	0.4643	2.7916	17.8	(100)	2.7989	3.15	0.0019
0	34.6786	0.5000	2.5846	16.7	(002)	2.5867	3.61	0.0021
	36.4286	0.5000	2.4644	16.7	(101)	2.4617	3.57	0.0021
	32.0714	0.4286	2.7886	19.3	(100)	2.7989	2.69	0.0018
3wt%	34.7143	0.6072	2.5821	13.7	(002)	2.5867	5.32	0.0025
	36.5357	0.4286	2.4574	19.5	(101)	2.4617	2.62	0.0018
	32.0357	0.4643	2.7916	17.8	(100)	2.7989	3.15	0.0019
5wt%	34.7143	0.4643	2.5821	17.9	(002)	2.5867	3.11	0.0019
	36.4286	0.4643	2.4644	18.0	(101)	2.4617	3.08	0.0019
	31.9543	0.5357	2.7985	15.4	(100)	2.7989	4.20	0.0022
7wt%	34.6786	0.6429	2.5846	13.0	(002)	2.5867	5.96	0.0027
	36.4200	0.3929	2.4650	21.3	(101)	2.4617	2.21	0.0016
	32.0357	0.4643	2.7916	17.8	(100)	2.7989	3.15	0.0019
9wt%	34.7143	0.3571	2.5821	23.3	(002)	2.5867	1.84	0.0015
	36.5000	0.4643	2.4597	18.0	(101)	2.4617	3.08	0.0019

UV–Visible–near-infrared spectrophotometer was used to record the optical transmission in the range of 300–1100 nm, for films with thickness 150 nm in the normal incident in this case as shown in Fig.3. The transmittance increases monotonically by increasing dopant atoms in the former and the best transmittance was found to be at (3wt%) however the transmittance reduced for high doping ratio.

A similar result was reported by Chabane et al. who observed a letdown in the transmission for an 8% doping, ratio [38]. This occurs by increasing the doping ratio which gives rise to structural enhancement.

The bandgap Eg was determined using Tauc formula [39]:

$$(\alpha h\nu)^{1/r} = B\,(h\nu - E_g^{opt}) \qquad (9)$$

where $h\nu$, E_g^{opt} and B are photon energy, optical band gap, and band tailing parameter, respectively, while r is a constant of 0.5 for direct permitted transition.

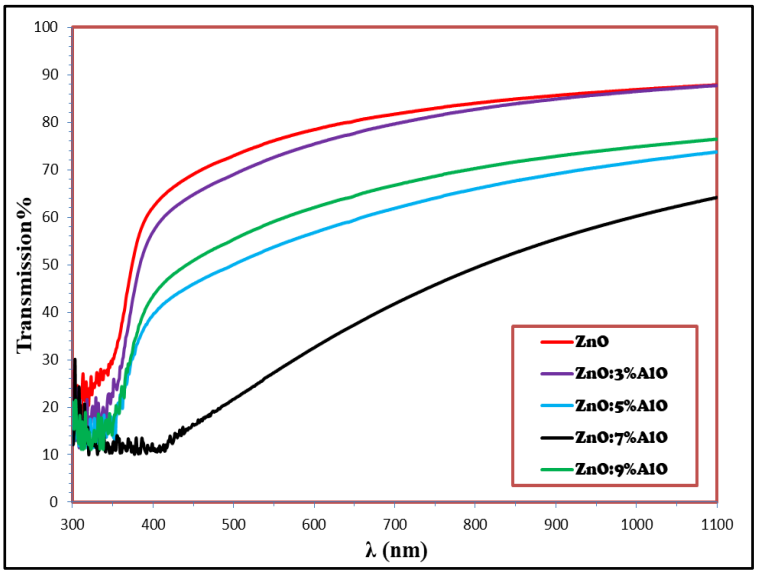

Figure 3: Transmittance spectra of ZnO: AlO thin films.

The optical band gap in Fig. 4 for both the undoped and the doped AlO thin films had same trend of transmittance i.e., it decreased monotonically by increasing the doping ratio up 7wt% and then started to increase. Mia et al. pointed out that optical band gaps of Al doped ZnO thin films showed increase from 3.30 to 3.37eV by increasing the doping ratio from 0 to 8mol% [40]. Bandgap shifts are the result of two competing factors.One is the bandgap narrowing and the other is the Burstein-Moss effect. The former happens when the donor and conduction bands overlap above a certain carrier concentration known as Mott density, which is around 4.5 10^{18} cm3. [41, 42] As the number of defects in the ZnO host matrix is high, the defect states become more delocalized and may overlap with the valence band edge, increasing it and reducing the banding distance [43]. While the latter occurs due to the increase of carrier concentration and the movement of Fermi level in the conduction band. It is found that transition metal dopants like (Mn, Co in $^{+2}$state,Fe) also increasethe bandgap of ZnO which is illustrated based on the exchange interaction of electrons in conduction and valence band with the d electrons of the dopants atoms [44, 46]. In terms of sp hybridization, as well [47]. The increase in bandgap occurred only on sample 9wt % AlO because stoichiometry is unchanged in pulsed laser deposition, which was used in this study, as a result, the concentration of dopant in the films was the same as in the starting content. The tunable band gap of the prepared thin films makes AlO doped ZnO thin films favorable for fabrication of heterojunction [48]. The refractive index n and the extinction coefficient k were determined from the relations [38]:

$$n = \left[\left(\frac{4R}{(R-1)^2} - k^2\right)\right]^{1/2} - \frac{(R+1)}{(R-1)} \qquad (10)$$

$$k = \frac{\alpha\lambda}{4\pi} \qquad (11)$$

where R the reflectanceand λ the wavelength of incident photon respectively n and k versus wavelength are shown in Figs.5 and 6, respectively. It was observed that n changed in a non-systematic sequence with increasing AlO dopant concentration. On the other hand, k increased by increasing dopant concentration while k falls for high doping concentration. It was found that maximum k value corresponded to the lowest bandgap value at 7wt% AlO. Table 2 The optical energy gap and optical constants are shown.

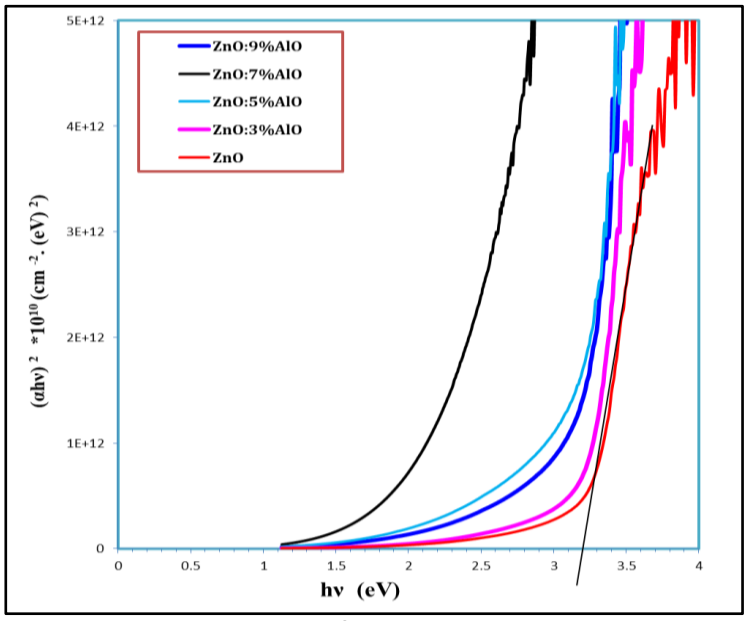

Figure 4: Variation of $(\alpha h\upsilon)^2$ with $(h\upsilon)$ of ZnO: AlO thin films.

Table 2: The optical energy gap and the optical constants at λ=550nm of thin ZnO: AlO films.

Sample	T%	α (cm^{-1})	k	n	ε_r	ε_i	Eg (eV)
ZnO	76.12	109162	0.478	2.062	4.025	1.972	3.21
ZnO:3%AlO	72.65	127817	0.560	2.160	4.353	2.418	3.2
ZnO:5%AlO	53.76	248263	1.087	2.566	5.405	5.580	3.1
ZnO:7%AlO	27.27	519787	2.276	2.355	0.364	10.719	2.1
ZnO:9%AlO	59.12	210264	0.921	2.478	5.293	4.563	3.21

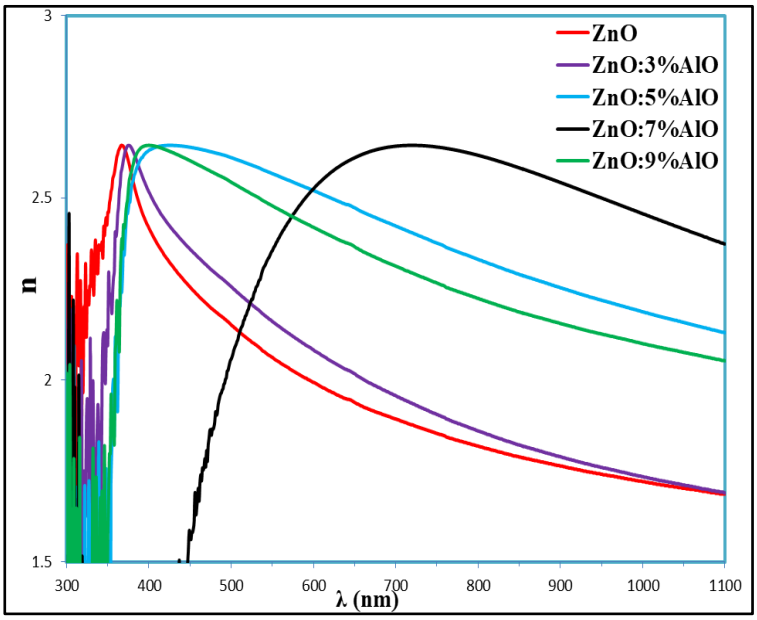

Figure 5: Refractive index spectra of ZnO: AlO thin films.

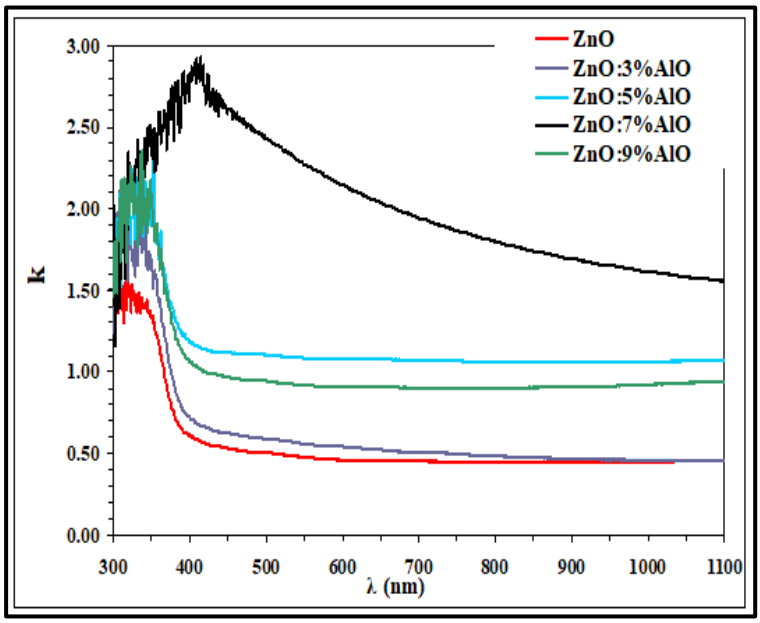

Figure 6: Extinction coefficient spectra of ZnO: AlO thin films.

Figures. 7 and 8 shows the changes of the Real and imaginary dielectric constants which were estimate by applying the following relations [48]:

$$\varepsilon_r = n^2 - k^2 \quad (12)$$

and

$$\varepsilon_i = 2nk \quad (13)$$

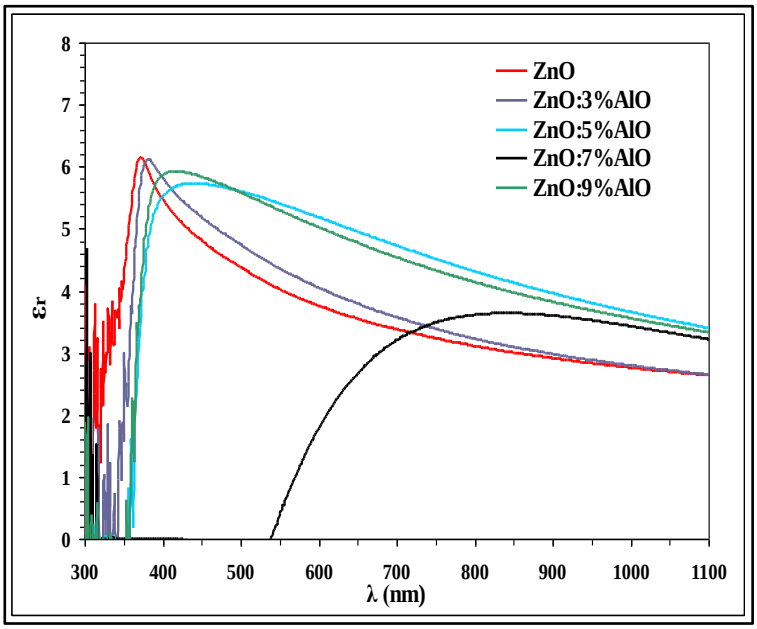

Figure 7: Real dielectric constant spectra of ZnO: AlO thin films.

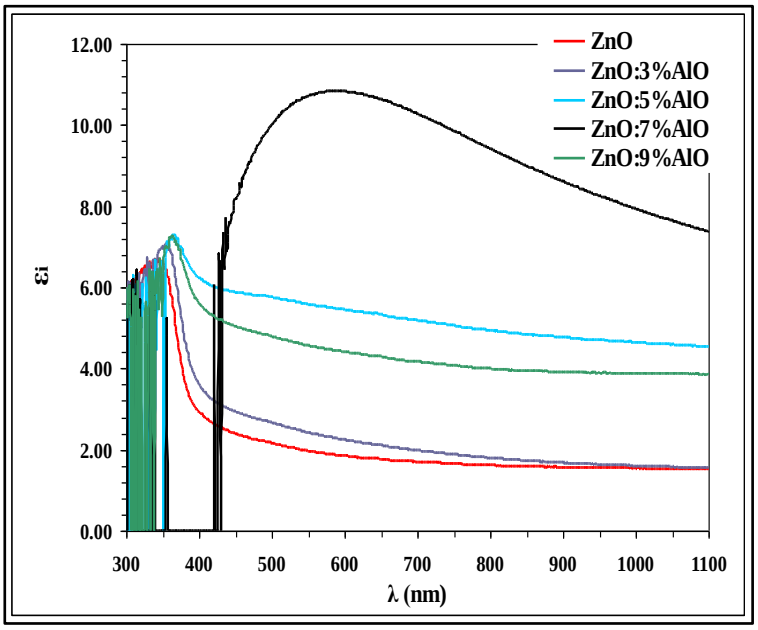

Figure 8: Imaginary dielectric constant spectra of ZnO: AlO thin films.

4. Conclusions

Nanocrystalline AlO doped ZnO thin films with hexagonal wurtzite of crystallite size inthe range of 15-19nm were prepared using pulsed laser deposition method with (100) as the predominant plane for crystal growth. The prepared thin films have transmittance in the range of 76-27%. The bandgap showed two different trends with increasing the doping ratio, the first was reduction of bang gap when the concentration of carriers exceeded that Mott density and widening of bandgap (Burstein-Moss effect). The ability to tune the bandgap by inserting a small number of dopant atoms makes the current films very appealing for optoelectronic system fabrication, such as light-emitting diodes.

Acknowledgments

The authors appreciate the cooperation they received from the chair of the Department of Physics and the University of Baghdad's College of Science's Department of Physics during the study process.

Conflict of interest

Authors declare that they have no conflict of interest.

References

1. Kim H., Gilmore a.C., Pique A., Horwitz J., Mattoussi H., Murata H., Kafafi Z., and Chrisey D., *Electrical, optical, and structural properties of indium–tin–oxide thin films for organic light-emitting devices.* Journal of applied physics, 1999. **86** (11): pp. 6451-6461.
2. Kim H., Gilmore C., Horwitz J., Pique A., Murata H., Kushto G., Schlaf R., Kafafi Z., and Chrisey D., *Transparent conducting aluminum-doped zinc oxide thin films for organic light-emitting devices.* Applied Physics Letters, 2000. **76**(3): pp. 259-261.
3. Kim H., Pique A., Horwitz J., Murata H., Kafafi Z., Gilmore C., and Chrisey D., *Effect of aluminum doping on zinc oxide thin films grown by pulsed laser*

deposition for organic light-emitting devices. Thin solid films, 2000. **377**: pp. 798-802.
4. Zhao J.-L., Li X.-M., Bian J.-M., Yu W.-D., and Gao X.-D., *Structural, optical and electrical properties of ZnO films grown by pulsed laser deposition (PLD).* Journal of Crystal Growth, 2005. **276**(3-4): pp. 507-512.
5. Das R. and Ray S., *Thickness dependence of the properties of magnetron sputtered ZnO: A1 films and its application in a-Si: H thin film solar cell.* Indian Journal of Physics, 2004. **78**: pp. 901-906.
6. He Y. and Kanicki J., *High-efficiency organic polymer light-emitting heterostructure devices on flexible plastic substrates.* Applied Physics Letters, 2000. **76**(6): pp. 661-663.
7. Lee S.-H., Han S.-H., Jung H.S., Shin H., Lee J., Noh J.-H., Lee S., Cho I.-S., Lee J.-K., and Kim J., *Al-doped ZnO thin film: a new transparent conducting layer for ZnO nanowire-based dye-sensitized solar cells.* The Journal of Physical Chemistry C, 2010. **114**(15): pp. 7185-7189.
8. Kaps S.r., Bhowmick S., Gröttrup J., Hrkac V., Stauffer D., Guo H., Warren O.L., Adam J., Kienle L., and Minor A.M., *Piezoresistive response of quasi-one-dimensional ZnO nanowires using an in situ electromechanical device.* Acs Omega, 2017. **2**(6): pp. 2985-2993.
9. Klingshirn C., *ZnO: From basics towards applications.* physica status solidi, 2007. **244**(9): pp. 3027-3073.
10. Jin X., Götz M ,.Wille S., Mishra Y.K., Adelung R., and Zollfrank C., *A novel concept for self-reporting materials: stress sensitive photoluminescence in ZnO tetrapod filled elastomers.* Advanced Materials, 2013. **25**(9): pp. 1342-1347.
11. Saji K.J., Tian K., Snure M., and Tiwari A., *2D tin monoxide—an unexplored p-type van der waals semiconductor: material characteristics and field effect transistors.* Advanced Electronic Materials, 2016. **2**(4): pp. 1500453.
12. Mishra Y.K., Kaps S., Schuchardt A., Paulowicz I., Jin X., Gedamu D., Freitag S., Claus M., Wille S., and Kovalev A., *Fabrication of macroscopically flexible and highly porous 3D semiconductor networks from interpenetrating nanostructures by a simple flame transport approach.* Particle Systems Characterization, 2013. **9**(30): pp. 775-783.
13. Reimer T., Paulowicz I., Röder R., Kaps S.r., Lupan O., Chemnitz S., Benecke W., Ronning C., Adelung R., and Mishra Y.K., *Single step integration of ZnO nano-and microneedles in Si trenches by novel flame transport approach: whispering gallery modes and photocatalytic properties.* ACS applied materials interfaces, 2014. **6**(10): pp. 7806-7815.
14. Shukla R., Srivastava A., Srivastava A., and Dubey K., *Growth of transparent conducting nanocrystalline Al doped ZnO thin films by pulsed laser deposition.* Journal of crystal growth, 2006. **294**(2): pp. 427-431.
15. Sarkar A., Ghosh S., Chaudhuri S., and Pal A., *Studies on electron transport properties and the Burstein-Moss shift in indium-doped ZnO films.* Thin Solid Films, 1991. **204**(2): pp.264-255 .
16. Bhosle V., Tiwari A., and Narayan J., *Electrical properties of transparent and conducting Ga doped ZnO.* Journal of Applied Physics, 2006. **100**(3): pp. 033713.
17. Sharma B.K. and Khare N., *Stress-dependent band gap shift and quenching of defects in Al-doped ZnO films.* Journal of Physics D: Applied Physics, 2010. **43**(46): pp. 465402.
18. Ohyama M., Kozuka H., and Yoko T., *Sol-gel preparation of transparent and conductive aluminum-doped zinc oxide films with highly preferential crystal*

orientation. Journal of the American Ceramic Society, 1998. **81**(6): pp. 1622-1632.
19. Lee J.-H. and Park B.-O., *Transparent conducting ZnO: Al, In and Sn thin films deposited by the sol–gel method.* Thin solid films, 2003. **426**(1-2): pp. 94-99.
20. Yamamoto Y., Saito K., Takahashi K., and Konagai M., *Preparation of boron-doped ZnO thin films by photo-atomic layer deposition.* Solar energy materials solar cells, 2001. **65**(1-4): pp. 125-132.
21. Sanchez-Juarez A., Tiburcio-Silver A., Ortiz A., Zironi E., and Rickards J ,. *Electrical and optical properties of fluorine-doped ZnO thin films prepared by spray pyrolysis.* Thin Solid Films, 1998. **333**(1-2): pp. 196-202.
22. Natsume Y. and Sakata H., *Electrical and optical properties of zinc oxide films post-annealed in H2 after fabrication by sol–gel process.* Materials Chemistry Physics, 2003. **78**(1): pp. 170-176.
23. Zhan Z., Zhang J., Zheng Q., Pan D., Huang J., Huang F., and Lin Z., *Strategy for preparing Al-doped ZnO thin film with high mobility and high stability.* Crystal growth design, 2011. **11**(1): pp. 21-25.
24. Mishra D., Srivastava A., Srivastava A., and Shukla R., *Bead structured nanocrystalline ZnO thin films: synthesis and LPG sensing properties.* Applied Surface Science, 2008. **255**(5): pp. 2947-2950.
25. Das A., Misra P., Bose A., Joshi S., Kumar R., Sharma T., and Kukreja L., *Structural, electrical and optical characteristics of Al doped ZnO films grown by sequential pulsed laser deposition.* Phys. Express, 2013. **3**(5).
26. .26Lu J., Fujita S., Kawaharamura T., Nishinaka H., Kamada Y., Ohshima T., Ye Z., Zeng Y., Zhang Y., and Zhu L., *Carrier concentration dependence of band gap shift in n-type ZnO: Al films.* Journal of Applied Physics, 2007. **101**(8): pp. 083705.
27. .27 Misra K.P., Shukla R., Srivastava A., and Srivastava A ,.*Blueshift in optical band gap in nanocrystalline Zn 1− x Ca x O films deposited by sol-gel method.* Applied Physics Letters, 2009. **95**(3): pp. 031901.
28. Das A., Misra P., and Kukreja L., *Effect of Si doping on electrical and optical properties of ZnO thin films grown by sequential pulsed laser deposition.* Journal of Physics D: Applied Physics, 2009. **42**(16): pp. 165405.
29. Yadav H.K. and Gupta V., *A comparative study of ultraviolet photoconductivity relaxation in zinc oxide (ZnO) thin films deposited by different techniques.* Journal of Applied Physics, 2012. **111**(10): pp. 102809.
30. Wu K.-Y., Wang C.-C., and Chen D.-H., *Preparation and conductivity enhancement of Al-doped zinc oxide thin films containing trace Ag nanoparticles by the sol–gel process.* Nanotechnology, 2007. **18**(30): pp. 305604.
31. Srivastava A., Kumar N., and Khare S., *Enhancement in UV emission and band gap by Fe doping in ZnO thin films.* Opto-Electronics Review, 2014. **22**(1): pp. 68-76.
32. Cullity B. and Stock S., *Elements of X-ray Diffraction, 3rd edn. Prentice Hall.* New York, 2001: pp. 174-177.
33. Srivastava A., Kumar N., Misra K.P., and Khare S., *Blue-light luminescence enhancement and increased band gap from calcium-doped zinc oxide nanoparticle films.* Materials science in semiconductor processing, 2014. **26**: pp. 259-266.
34. Lee J.-H. and Park B.-O., *Characteristics of Al-doped ZnO thin films obtained by ultrasonic spray pyrolysis: effects of Al doping and an annealing treatment.* Materials Science Engineering: B, 2004. **106**(3): pp. 24.245-2

35. Zhou H.-m., Yi D.-q., Yu Z.-m., Xiao L.-r., and Li J., *Preparation of aluminum doped zinc oxide films and the study of their microstructure, electrical and optical properties.* Thin solid films, 2007. **515**(17): pp. 6909-6914.
36. Chen K.-J., Fang T.-H., Hung F.-Y., Ji L.-W., Chang S.-J., Young S.-J., and Hsiao Y., *The crystallization and physical properties of Al-doped ZnO nanoparticles.* Applied surface science, 2008. **254**(18): pp. 5791-5795.
37. Venkatachalam S., Iida Y., and Kanno Y., *Preparation and characterization of Al doped ZnO thin films by PLD.* Superlattices Microstructures, 2008. **44**(1): pp. 127-135.
38. Chabane L., Zebbar N., Kechouane M., Aida M., and Trari M., *Al-doped and in-doped ZnO thin films in heterojunctions with silicon.* Thin Solid Films, 2016. **605**: pp. 57-63.
39. Tauc J., *Optical Properties of Solids, ed.* F. Abeles, NorthHolland, Amsterdam, 1970. **22**: pp. 903.
40. Mia M., Habiba U., Pervez M., Kabir H., Nur S., Hossen M., Sen S., Hossain M.K., Iftekhar M.A., and Rahman M.M., *Investigation of aluminum doping on structural and optical characteristics of sol–gel assisted spin-coated nano-structured zinc oxide thin films.* Applied Physics A, 2020. **126**(3): pp. 1-12.
41. Kumar J. and Kumar Srivastava A., *Band gap narrowing in zinc oxide-based semiconductor thin films.* Journal of Applied Physics, 2014. **115**(13): pp. 134904.
42. Saw K., Aznan N., Yam F., Ng S., and Pung S., *New insights on the burstein-moss shift and band gap narrowing in indium-doped zinc oxide thin films.* PloS one, 2015.**10**(10): pp. e0141180.
43. Wang J., Wang Z., Huang B., Ma Y., Liu Y., Qin X., Zhang X., and Dai Y., *Oxygen vacancy induced band-gap narrowing and enhanced visible light photocatalytic activity of ZnO.* ACS applied materials interfaces, 2012. **4**(8): pp. 4024-4030.
44. Bylsma R., Becker W., Kossut J., Debska U., and Yoder-Short D., *Dependence of energy gap on x and T in Zn 1− x Mn x Se: the role of exchange interaction.* Physical Review B, 1986. **33**(12): pp. 8207.
45. Fukumura T., Jin Z., Ohtomo A., Koinuma H ,.and Kawasaki M., *An oxide-diluted magnetic semiconductor: Mn-doped ZnO.* Applied physics letters, 1999. **75**(21): pp. 3366-3368.
46. Furdyna J.K., *Diluted magnetic semiconductors.* Journal of Applied Physics, 1988. **64**(4): pp. R29-R64.
47. Pankove J.I., *Optical processes in semiconductors*. 1975: Dover Publications, Inc., New York.
48. Fentahun D.A., Tyagi A., and Kar K.K., *Numerically investigating the AZO/Cu2O heterojunction solar cell using ZnO/CdS buffer layer.* Optik, 2021. **228**: pp. 166228.

تأثير محتوى أوكسيد الألمنيوم على الخواص التركيبية والبصرية لاغشية ZnO: AlO الرقيقة

حوراء هادي عباس، بشرى عباس حسن
قسم الفيزياء، كلية العلوم، جامعة بغداد، بغداد، العراق

الخلاصة

يتم تصنيع الأغشية الرقيقة البلورية النانوية من اوكسيد الزنك المطعم باوكسيد الالمنيوم بحجم بلوري ضمن المدى (15-19 نانومتر) عن طريق الترسيب بالليزر النبضي. ان هبوط حجم البلورات مع زيادة نسبة التطعيم ادى الى زحف فجوة الطاقة الى المنطقة تحت الحمراء. لقد هبطت فجوة الطاقة البصرية وبانتظام من 3.21 إلى 2.1 eV عن طريق زيادة نسبة تطعيم من 0 إلى 7% ولكنها تعود بعد ذلك للنمو حتى 3.21 eV من خلال استمرار الزيادة في نسبة التطعيم. ان زيادة فجوة الطاقة و التي تم الحصول عليها عند نسبة التطعيم 9% يمكن توضيحة من خلال تأثير بورشتاين-موس حيث تزيد ذرة الألمنيوم المانحة من تركيز حاملات الشحنة والذي بدوره يزحف مستوى فيرمي ويوسع فجوة الطاقة (الانحراف نحو الأزرق). ان امكانية هندسة فجوة الطاقة ولقيم واطئة من التطعيم باوكسيد الالمنيوم AlO تجعل الأغشية الرقيقة :ZnO مفضلة لتصنيع النبائط الكهرو - بصرية. كما تم حساب الثوابت البصرية والتي وجد انها تتأثر كثيرا بزيادة نسبة التطعيم.